

Article

Effect of the Ultrasonic Nanocrystalline Surface Modification (UNSM) on Bulk and 3D-Printed AISI H13 Tool Steels

In-Sik Cho ¹, Chang-Soon Lee ¹, Chang-Ha Choi ¹, Hyung-Gyu Lee ², Moon Gu Lee ²
and Yongho Jeon ^{2,*} 

¹ Department of Advanced Material Engineering, Sun Moon University, 70, Sunmoon-ro 221 beon-gil, Tangjeong-myeon, Asan-si, Chungcheongnam-do 31460, Korea; mbrosia1018@naver.com (I.-S.C.); lcs8769@sunmoon.ac.kr (C.-S.L.); chchoi@sunmoon.ac.kr (C.-H.C.)

² Department of Mechanical Engineering, Ajou University, 206 Worldcup-ro, Yeongtong-gu, Suwon 16499, Korea; eric@leetech-kr.com (H.-G.L.); moongulee@ajou.ac.kr (M.G.L.)

* Correspondence: princaps@ajou.ac.kr; Tel.: +82-31-219-3652

Received: 18 October 2017; Accepted: 17 November 2017; Published: 21 November 2017

Abstract: A comparative study of the microstructure, hardness, and tribological properties of two different AISI H13 tool steels—classified as the bulk with no heat treatment steel or the 3D-printed steel—was undertaken. Both samples were subjected to ultrasonic nanocrystalline surface modification (UNSM) to further enhance their mechanical properties and improve their tribological behavior. The objective of this study was to compare the mechanical properties and tribological behavior of these tool steels since steel can exhibit a wide variety of mechanical properties depending on different manufacturing processes. The surface hardness of the samples was measured using a micro-Vickers hardness tester. The hardness of the 3D-printed AISI H13 tool steel was found to be much higher than that of the bulk one. The surface morphology of the samples was characterized by electron backscattered diffraction (EBSD) in order to analyze the grain size and number of fractions with respect to the misorientation angle. The results revealed that the grain size of the 3D-printed AISI H13 tool steel was less than 0.5 μm , whereas that of the bulk tool steel was greater than 4 μm . The number of fractions of the bulk tool steel was about 0.5 μm at a low misorientation angle, and it decreased gradually with increasing misorientation angle. The low-angle grain boundary (LAGB) and high-angle grain boundary (HAGB) of the bulk sample were about 21% and 79%, respectively, and those of the 3D-printed sample were about 8% and 92%, respectively. Moreover, the friction and wear behavior of the UNSM-treated AISI H13 tool steel specimen was better than those of the untreated one. This study demonstrated the capability of 3D-printed AISI H13 tool steel to exhibit excellent mechanical and tribological properties for industrial applications.

Keywords: AISI H13 steel; UNSM; 3D printing; hardness; grain size; wear

1. Introduction

AISI H13 tool steel is a Cr-Mo hot work steel with a wide range of tooling applications in hot and cold work such as in extrusion tools, pressure die casting tools, forging dies, hot shear blades, plastic mold cavities, industrial knives, shot sleeves, and tools in various industries owing to its properties such as high hardenability, excellent wear resistance, and good thermal shock resistance [1,2]. The hardness of AISI H13 tool steel can resist the thermal fatigue cracking that occurs as a result of cyclic heating and cooling processes. AISI H13 tool steel is an excellent material for use in hot work tooling—better than other tool steels—because of its high toughness and high resistance to thermal fatigue cracking. Therefore, its mechanical properties and wear resistance need to be enhanced

to extend the fatigue life span of mechanical components and dies made of AISI H13 tool steel. Moreover, from an economic point of view, it is necessary to make those parts lighter, while maintaining or improving characteristics such as the mechanical, physical, chemical, and tribological properties. In general, materials are subjected to heat treatment in order to improve their mechanical properties. The hardness of AISI H13 tool steel after quenching is in the range of 48–50 HRC. Mo and V serve as strengthening agents, while Cr assists in increasing the resistance of AISI H13 tool steel to softening at high temperatures.

In recent years, additive manufacturing, especially metal 3D printing, has attracted considerable attention due to its emerging properties such as the minimization of material use, the ability to build any complex shape with a light structure, and the reduction in cost for the manufacturing of mechanical components with reduced energy [3–5]. The structure built by layer-by-layer processing of metal 3D printing can compete with bulk materials in terms of mechanical and physical properties for mass adoption. It has been reported that 3D-printed mechanical components can be up to 60% lighter than machined mechanical components [6]. In this regard, the emerging technology of 3D printing is in high demand because of the economic aspect, owing to the aforementioned unique properties offering both product complexity and multifunctionality of new materials. For example, the aerospace industry alone saves billions of dollars by weight reduction of mechanical components [7]. Currently, some 3D printing technologies allow printing multiple materials simultaneously [8], which is an excellent achievement in the metal 3D printing field. Moreover, 3D printing technology has gradually achieved levels of accuracy and precision that can be deemed somewhat satisfactory [9]. However, there remain some issues related to the final product produced by the metal 3D printing process. One of the major issues of metal 3D printing in terms of mechanical properties is the presence of micro-pores, which occur in mechanical components cracked under cyclic loading, where the porosity locations act as sites for crack initiation, nucleation, and propagation. The relationship between the microstructure defects and mechanical properties of materials is very important since the final wear, fatigue, and corrosion properties of materials can be determined by surface and microstructure defects such as cracks, pores, and unmelted particles [10]. It has been reported earlier that 3D-printed AISI H13 tool steel manufactured by different additive manufacturing methods has a lower fatigue strength owing to the detrimental effects of porosity [11].

A number of heat treatment and surface engineering methods can eliminate pores and enhance the mechanical properties of materials in order to improve the resistance to wear and fatigue lifespan of overall mechanical components. For example, hot isostatic pressure (HIP) is usually employed to eliminate the internal pores formed during manufacturing as well as to improve the mechanical properties of materials. AlMangour et al. investigated the influence of HIP post-treatment of AISI H13 tool steel manufactured by the selective laser melting (SLM) method [12]. Moreover, a number of severe plastic deformation (SPD) methods have also been widely used to improve the mechanical properties of materials by generating a severe plastically deformed layer with a thickness of more than 100 μm [13,14]. The main mechanism of the enhancement in mechanical properties of materials subjected to SPD methods involves the presence of the nanocrystal structure with refined grains at the nanoscale [15]. Cho et al. studied the surface hardening of AISI H13 tool steel by shot peening and concluded that the surface hardening occurred for the refined grains, as confirmed by transmission electron microscopy (TEM) images [16].

In this study, therefore, we employed a relatively newly developed alternative ultrasonic nanocrystal surface modification (UNSM) process to further improve the mechanical properties and tribological behavior of 3D-printed AISI H13 tool steel. This process increases the surface hardness, reduces the surface roughness, and refines the coarse grains into nano-size grains [17], thus improving the friction and wear behavior and fatigue lifespan of materials. A comparative study of the microstructure, hardness, friction and wear, and scratching resistance of bulk AISI H13 tool steel with no heat-treatment and 3D-printed AISI H13 tool steel was undertaken. The UNSM treatment

demonstrated the capability of increasing the surface hardness and friction and wear behavior of 3D-printed AISI H13 tool steel, which can be used in various tooling applications.

2. Experimental Procedure

2.1. Direct Metal Tooling and Specimen Preparation

An AISI H13 tool steel specimen with a bar shape was selected as the base material that was not pre-treated by a quenching and tempering heat-treatment process, as our aim was to compare the properties of the bulk specimen with the 3D-printed specimen not subjected to a heat treatment process since no additional heat treatment process is undertaken after the metal 3D printing process. An AISI H13 tool steel sample was manufactured by metal 3D printing using a laser-aided direct metal tooling (DMT) machine (MX-450, InssTak Inc., Daejeon, Korea) using a 1 kW ytterbium fiber laser. In this method, laser energy melts powder metals in an enclosed chamber and repeats the process by layer until the construct is fully realized; this process is similar to the laser cladding or thermal spray processes. DMT is an additive manufacturing process that can be used for rapid prototyping, tooling, and functional part fabrication with specific metals. The process fabricates structures by building the layers. The layers are deposited on preceding layers by local melting of the feeding powder under the high-power laser and the flow of an inert gas [18]. The rapid heating, melting, and cooling of feeding powders can generate the following results: (1) distortion and dimensional inaccuracy, (2) high residual stresses on the parts, (3) local cracks by thermal shock, and (4) voids that can deteriorate the mechanical properties [19]. DMT can be applied to various metal powders, but this study focused on AISI H13 tool steel. Conventional H13 steel is a martensitic steel alloy that can offer high hardenability, excellent wear resistance, and hot toughness. However, DMT-processed AISI H13 tool steel experiences quick melting, cooling, and reheating. Therefore, its material properties cannot be the same as the conventional one. Additionally, the laser process direction and voids are also affected.

The material was cut into a plate-shaped specimen with dimensions of $10 \times 10 \times 3 \text{ mm}^3$ using wire cutting with a wire diameter of 0.14 mm to avoid any generation of stress and change in the microstructure that might be induced by heat generation. The chemical composition and mechanical properties of the specimens are listed in Tables 1 and 2, respectively. The yield strength, ultimate tensile strength, and elongation of the specimens were assessed using a tensile test, while the elastic modulus was evaluated using a nanoindentation. The chemical composition was obtained using energy-dispersive X-ray spectroscopy (EDX, AMETEK, Mahwah, NJ, USA). The specimens were polished using several levels of silicon carbide (SiC) sandpaper up to #2000 grit in order to achieve a relatively similar average surface roughness with a value of about $>0.1 \text{ }\mu\text{m}$. A mirror-like surface for surface characterization was obtained using a 1- μm diamond suspension.

Table 1. Chemical composition of the bulk and 3D-printed AISI H13 tool steel in wt. %.

Material	C	V	Si	Mo	Mn	Cr	Fe
Bulk	0.32	1.00	1.00	1.33	0.25	5.13	balance
3D-printed	0.41	0.90	1.00	1.40	0.35	5.35	balance

Table 2. Mechanical properties of the bulk and 3D-printed AISI H13 tool steel.

Material	Yield Strength, MPa	Elastic Modulus, GPa	UTS, GPa	Elongation, %
Bulk	1650 ± 24.64	210 ± 3.44	1990 ± 28.34	9 ± 0.63
3D-printed	1720 ± 24.99	218 ± 3.35	2010 ± 29.67	12 ± 0.66

2.2. UNSM Technique

The UNSM technique strikes the top surface of the specimen to refine the grains into nano-size grains with a 2.38-mm diameter WC/Si₃N₄ tip at a frequency of 20 kHz [20]. Figure 1 shows the

schematic of the experimental setup. In the UNSM process, a generator and piezoelectric transducer produce 20 kHz waves, and this is amplified at the booster. The tip, which is already in contact with the surface, vibrates with amplitudes in the range of 10–100 μm . For this reason, a static load (P_{st}) and dynamic load ($P_{dy} = P \sin 2\pi ft$) is applied and results in a homogeneous treatment on the surface.

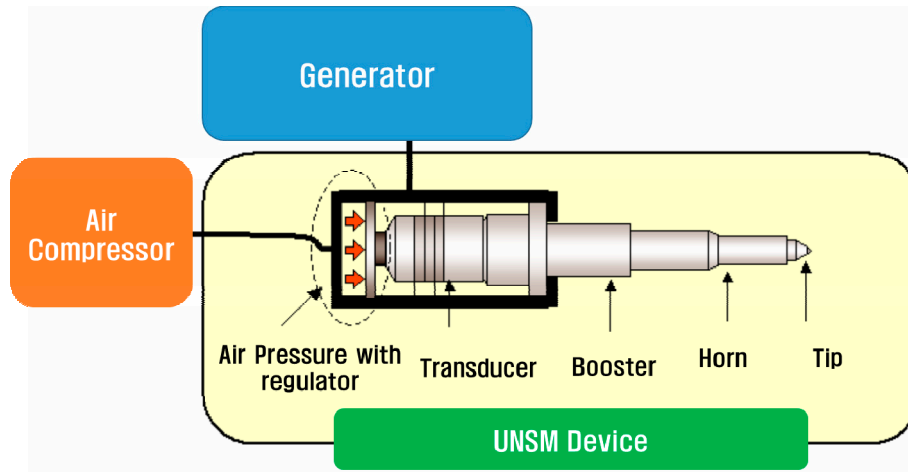


Figure 1. Ultrasonic fatigue tester.

The basic concept of UNSM is the instrumental conversion of acoustically tuned harmonic oscillation into ultrasonically resonant impulses. The UNSM system can be installed onto conventional NC/CNC machines. In this study, the UNSM treatment was performed on an NC lathe with a piezoelectric-actuated precise tool positioning stage.

The specimens were treated with the optimized parameters listed in Table 3, which were selected based on several experimental results in term of surface integrity and surface condition. As can be seen in Table 3, the applied static loads of the bulk and 3D-printed AISI H13 tool steel specimens were 30 and 70 N owing to the difference in the initial surface hardness of the specimens, respectively. Further details of the UNSM technique have been provided in previous publications [21,22]. Prior to the UNSM treatment, the specimens were cleaned with ethanol and deionized water for 10 min each using an ultrasonic bath to keep the surface clean, without dust or particles.

Table 3. Optimized ultrasonic nanocrystalline surface modification (UNSM) treatment parameters for bulk and 3D-printed AISI H13 tool steel.

Material	Frequency, kHz	Amplitude, μm	Static Load, N	Speed, mm/min	Feed Rate, μm	Ball Diameter, mm	Ball Material
Bulk	20	30	30	2000	70	2.38	WC
3D-printed			70				

2.3. Friction and Wear Test

The friction and wear behavior of the AISI H13 tool steel specimens was assessed using a ball-on-disk micro-tribo tester (CSM Instruments, Peseux, Switzerland) under dry conditions at room temperature under the test conditions listed in Table 4. The specimens were subjected to friction and wear tests under the same test conditions. A bearing steel (SAE52100) ball with a diameter of 12.7 mm was used as a counter surface specimen, which was fixed to the specimen holder, while the lower AISI H13 tool steel specimen reciprocated back and forth. A schematic view of the ball-on-disk setting configuration is shown in Figure 2. The tests were replicated at least three times to obtain a standard deviation and the mean values of three or more test results are reported here. The three different cross-sectional wear track profiles were examined to quantify the wear area. The specific wear rate

and corresponding standard deviation of the specimens were computed as the ratio of wear volume loss over the normal load multiplied by the total reciprocating sliding distance.

Table 4. Friction and wear test conditions.

Material	Applied Load, N	Contact Stress, GPa	Reciprocating Speed, cm/s	Reciprocating Time, min	Stroke, mm
Bulk 3D-printed	10	0.6	2.51	60.0	2.0

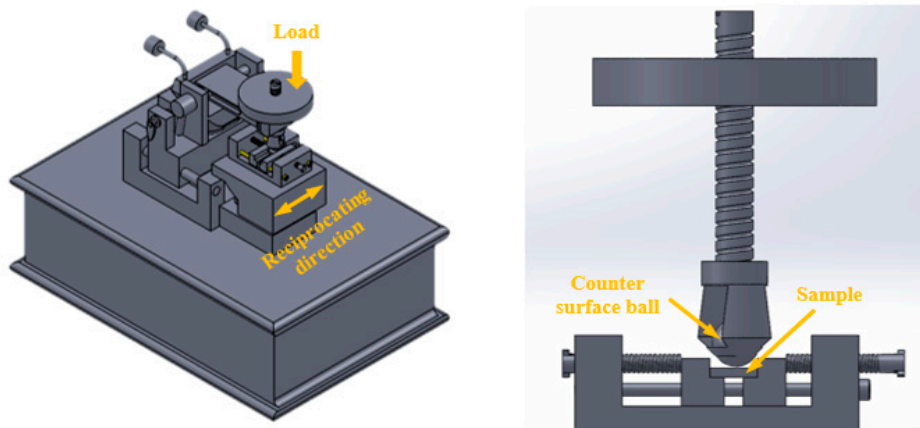


Figure 2. Schematic view of a ball-on-disk setting configuration.

2.4. Scratch Test

The micro-scratch behavior of the untreated and UNSM-treated AISI H13 tool steel specimens was evaluated using a single stroke micro-scratch tester (CSM Instruments, Peseux, Switzerland) equipped with a Rockwell diamond conical probe with a hemispherical tip radius of 200.0 μm at a progressive load from 0.0 to 50.0 N and a scratch speed of 20.0 mm/min over a total scratch length of 3.0 mm. All scratches were repeated three times in the same direction and the average data are reported in this study. The applied progressive load and frictional force were recorded during scratching. The friction coefficient was calculated based on the ratio of progressive load to friction force. Scratch grooves were generated by the plastic deformation of the surface during scratching.

2.5. Characterization Tools

The average surface roughness, which was controlled to be similar by polishing in order to avoid its effect on the friction and wear behavior of the AISI H13 tool steel specimens, was measured using a two-dimensional surface profilometer (Mitutoyo SJ-210, Mitutoyo, Kawasaki, Japan). The surface hardness was measured using a microhardness tester (Mitutoyo MVK E3, Mitutoyo, Kawasaki, Japan) at a load of 300 gf and a dwell time of 10 s. Surface morphology, wear tracks, and scratch grooves were characterized using scanning electron microscopy (SEM; JEOL JSM-7000F, JEOL, Tokyo, Japan). The cross-sections of the wear track profile were measured by non-contact 3D laser scanning microscopy (VK-X100 Series, Keyence, Osaka, Japan). The chemical compositions before and after wear tests were determined using an EDX (EDAX, AMETEK, Mahwah, NJ, USA). The microstructural evolution and grain size of the specimens were characterized by using an electron backscattered diffraction (EBSD) (JSM-7100F, JEOL, Tokyo, Japan) device attached to an SEM.

3. Results

3.1. Microstructural Evolution

Figure 3 shows the surface morphology along with mapping of the as-received and 3D-printed specimens obtained using EBSD. It can be seen from Figure 3a that the average grain size of the as-received specimen was in the range of 5–30 μm in the longitudinal direction. It is clear from Figure 3b that the UNSM treatment refined the coarse grains into very fine grains with sizes in the range of 1–10 μm in the longitudinal direction. The grain size refinement of the UNSM-treated specimen can be recognized to the continuous striking during treatment, which induced severe plastic deformation at the top surface up to a certain depth. In the case of the 3D-printed specimens, as shown in Figure 3c,d, the grain size spanned a large range; among the coarse grains, the presence of refined grains could be observed, owing to the heating during additive manufacturing. Those coarse grains were further refined by the UNSM treatment, owing to which the average grain size was found to be less than 50 nm. It has been previously reported that the UNSM technique is able to produce a nanostructured material with a grain size of less than 100 nm [23]. The grain size refinement by UNSM treatment can be attributed to SPD, where dislocation accumulation occurs first and then sub-grains are formed. Afterwards, some dislocations are annihilated at the sub-grain boundaries to increase the misorientation angles. Finally, a balance between the formation of dislocations by SPD and the absorption of dislocations at grain boundaries is established [24]. The number of grain boundaries significantly increases because of the refinement of coarse grains into nano-grains [25]. Moreover, it can be proposed that a large number of dislocations are formed in the grain, and dislocations are rearranged in order to lower the energy level, and a large number of low grain boundaries are formed during UNSM treatment.

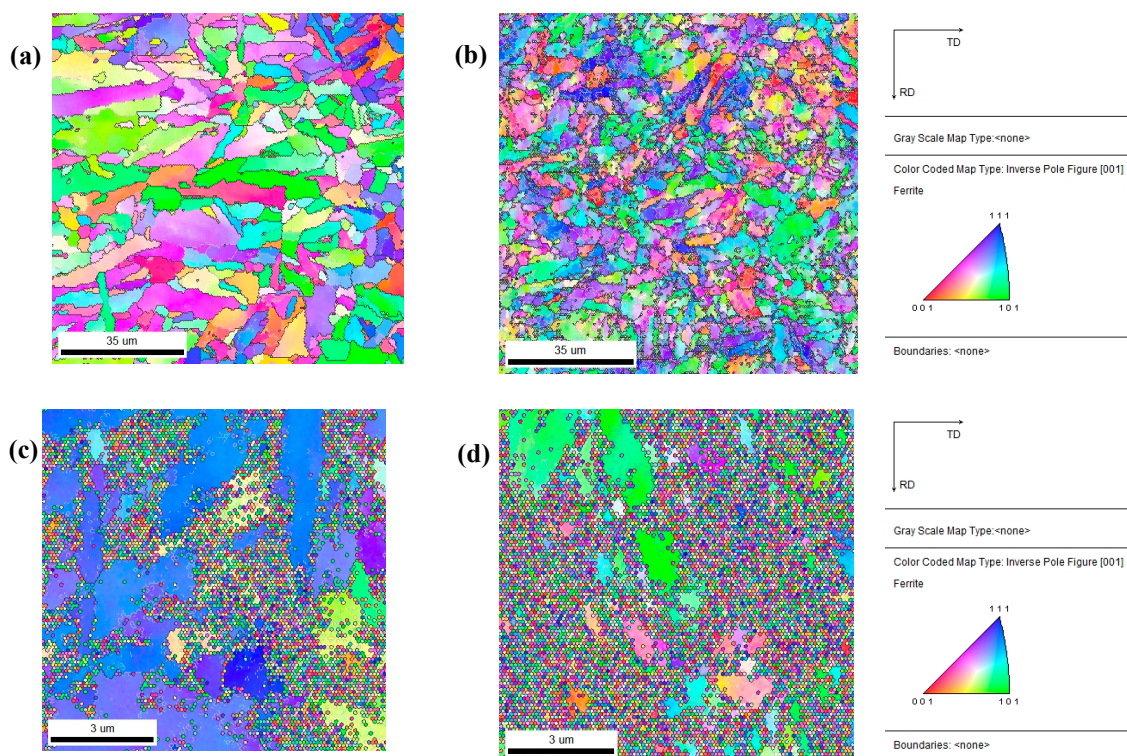


Figure 3. EBSD (electron backscattered diffraction) images along with mapping of the bulk (a,b) and 3D-printed (c,d) AISI H13 tool steel specimens before and after UNSM treatment.

The number of fractions with respect to the misorientation angle of the as-received and 3D-printed specimens obtained using EBSD is shown in Figure 4. In the case of the bulk specimens, as shown in

Figure 4a,b, the number of fractions of the specimens after UNSM treatment increased. The amount of low-angle grain boundary (LAGB) also increased from 21% to 34%, whereas the amount of high-angle grain boundary (HAGB) decreased from 79% to 66%. In the case of the 3D-printed specimens shown in Figure 4c,d, the amount of LAGBs also increased from 8% to 17%, while the amount of HAGBs decreased from 92% to 83%. This change in grain boundaries may be attributed to the increased number of grain boundaries owing to UNSM treatment [26]. As a result of the grain refinement, mechanical properties such as the hardness of materials can improve significantly. The following sub-section describes the increase in the surface hardness and the decrease in the surface roughness after UNSM treatment.

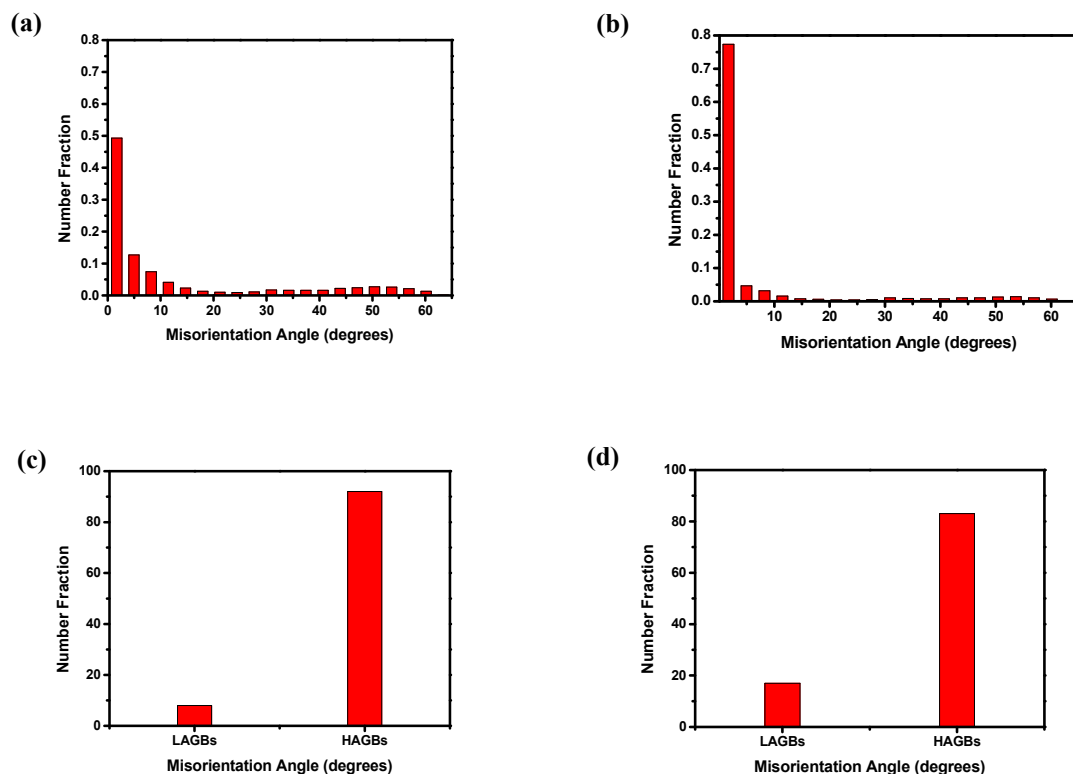


Figure 4. Number of fractions with respect to the misorientation angle for the bulk (a,b) and 3D-printed (c,d) AISI H13 tool steel specimens before and after UNSM treatment.

3.2. Surface Roughness and Surface Hardness

Surface roughness of the untreated and UNSM-treated specimens was measured as shown in Figure 5. It was evident that the average surface roughness of the bulk specimen increased after UNSM treatment from 0.445 to 0.563 μm , while no significant difference was observed for the average surface roughness for the 3D-printed untreated and UNSM-treated specimens, with observed values of 0.451 and 0.454 μm , respectively. Figure 5b shows that the UNSM treatment tracks were clearly generated on the specimen surface with a distance (feed-rate) of 70 μm , as shown in Table 3. This corrugated surface was generated by the forward and backward movement of UNSM treatment during processing. The top surface images of the untreated and UNSM-treated specimens confirmed that the UNSM treatment resulted in the formation of micro-dimples on the specimen surface. Some surface modification technologies can produce a micro-dimple on the surface that has a beneficial effect on the tribological properties of the material. For example, desired micro-dimples can be produced by laser surface texturing (LST) technology [27], but the resultant size of micro-dimples is greater than that produced by UNSM treatment [28].

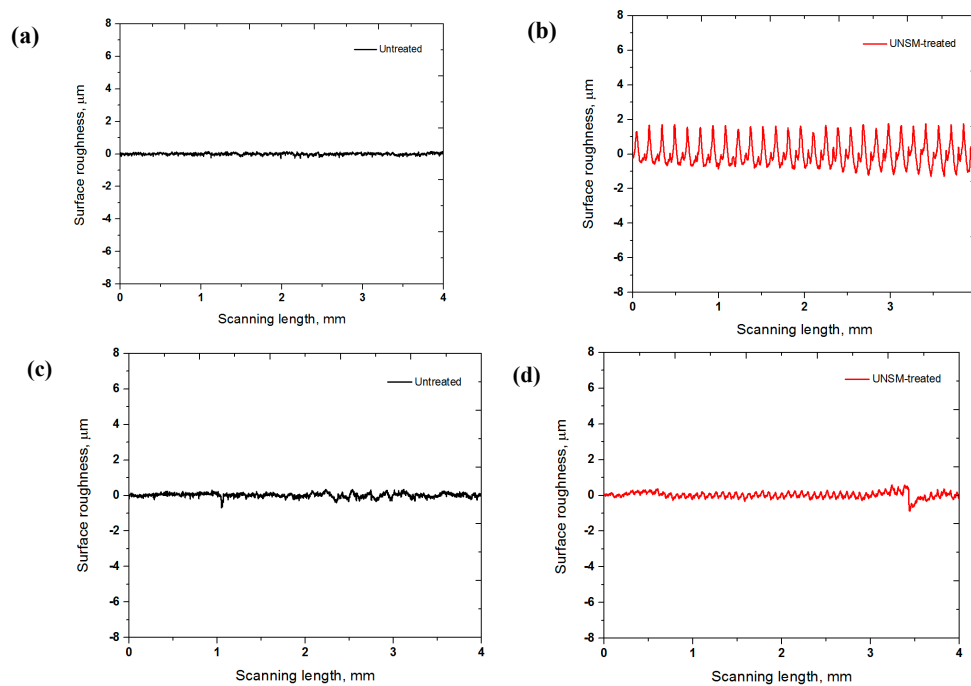


Figure 5. Comparison of surface roughness of the bulk (a,b) and 3D-printed (c,d) AISI H13 tool steel specimens before and after UNSM treatment.

The surface hardness of the specimens before and after UNSM treatment was measured to investigate the effects of grain refinement after UNSM treatment on the surface hardness; the comparison of the surface hardness values is shown in Figure 6. It can be seen that both the UNSM-treated specimens exhibited a significantly high hardness in comparison with that of the as-received and 3D-printed specimens. The surface hardness of the as-received and UNSM-treated bulk and 3D-printed specimens increased from 21 to 34 HRC and 60 to 65 HRC, respectively. It is important to note that the 3D-printed specimens had a higher hardness in comparison with the bulk ones, which were not heat-treated, because of the increase in temperature during the build-up of a material by means of the inert gas (either argon or nitrogen at oxygen levels below 500 parts per million) to reach a higher melting temperature [29]. The difference between the indentation size of both the specimens before and after UNSM treatment is shown in Figure 7. The refined grains after UNSM treatment were directly responsible for the increase in the surface hardness, which can be explained by the Hall-Petch relationship [30]. A previous study found by TEM observation that the increase in the surface hardness could also be recognized to the high dislocation density and increased area fraction of the grain boundaries [31].

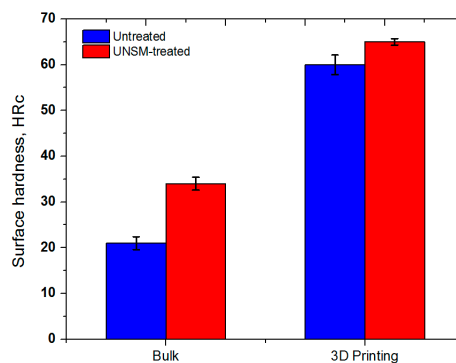


Figure 6. Comparison of surface hardness of the bulk and 3D-printed AISI H13 tool steel specimens before and after UNSM treatment.

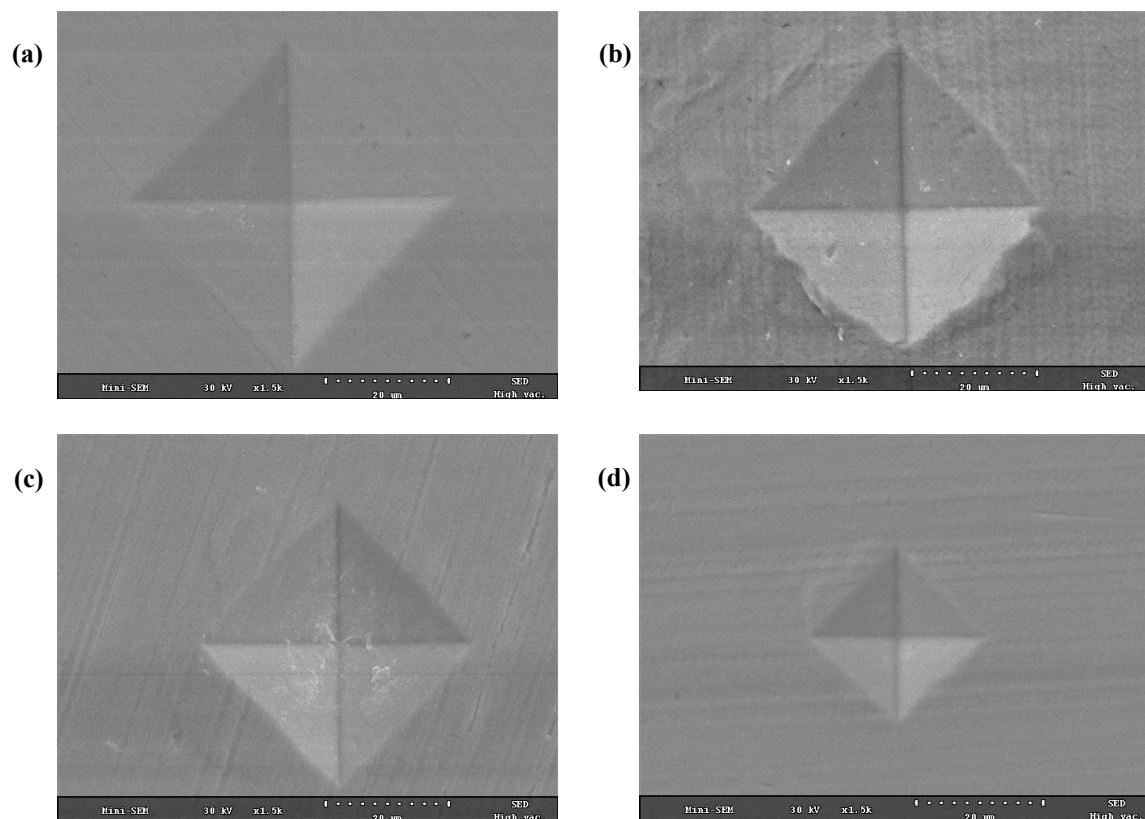


Figure 7. SEM images of an indent on the bulk (a,b) and 3D-printed (c,d) AISI H13 tool steel specimens before and after UNSM treatment.

3.3. Friction and Wear Behavior

Dry sliding friction tests were conducted on the bulk and 3D-printed UNSM untreated and treated specimens to investigate the influence of the UNSM treatment on the friction and wear behavior. Figure 8 shows the friction behavior of the specimens with respect to the sliding time for up to 70 min. It was found that the UNSM-treated specimen showed a lower friction coefficient than the untreated one in both cases. In the case of the bulk specimens, the friction coefficient increased rapidly at the beginning of sliding due to surface contamination (e.g., water absorption) and initial contact. After reaching the highest point, it decreased gradually with time and reached a plateau at 0.41 and 0.36 for the untreated and UNSM-treated bulk specimens, respectively. The friction coefficients of the untreated specimen in the running-in and steady-state periods were found to be higher than those of the UNSM-treated specimen by about 14%. For the 3D-printed specimens, the friction coefficient increased rapidly at the onset of sliding, where the UNSM-treated specimen showed a higher decrease rate than the untreated one by about 20%, which may be attributed to the presence of the corrugated surface, resulting in a decrease in the contact area at the interface [32]. Moreover, the yield strength increase requires more energy for plastic deformation and reduces the friction coefficient of the UNSM-treated specimens [33]. The short period of high friction behavior for the untreated specimen at the beginning of the test may be affected by the smoothing of the initial surface roughness. However, the friction behavior was relatively stable with little fluctuation. In contrast, the friction behavior of the UNSM-treated specimen started fluctuating in the transition period from the running-in stage to the steady-state stage. This friction behavior usually occurs because of the initial surface roughness and the plastic deformation of contact interface by high contact stress [34]. In other words, the repeated sliding causes the contact area increase and results in the formation of a wear track on the

surface. The friction coefficient decrease of the UNSM-treated specimen causes a change in the surface roughness and results in a surface modified by UNSM [35].

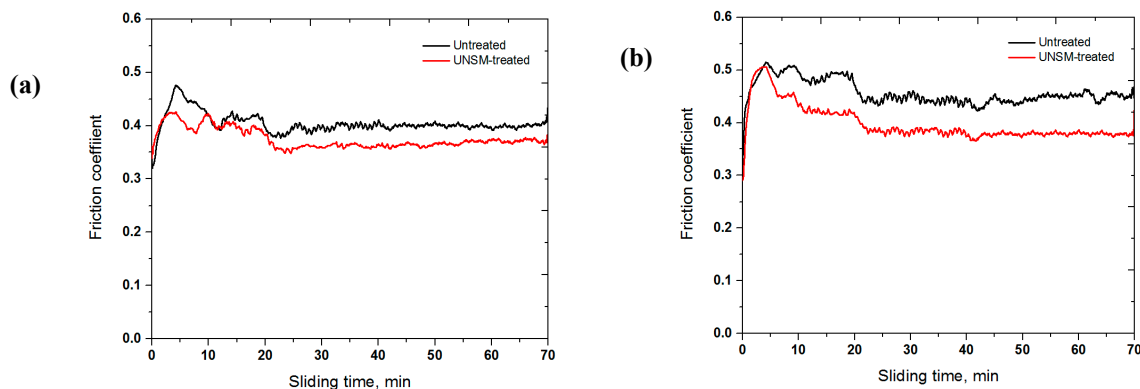


Figure 8. Comparison of friction coefficients of the bulk (a) and 3D-printed (b) AISI H13 tool steel specimens before and after UNSM treatment.

Figure 9 shows the wear track images of the untreated and UNSM-treated bulk and 3D-printed specimens. The SEM images show that the surface wear track was different between UNSM-treated and untreated specimen. In addition, significant changes were noted in the surface roughness of the specimens after the friction test. However, for the UNSM-treated specimen, the wear track was partially formed because of the corrugated surface, which does not allow the specimen to have full contact with the counter surface. In the case of the untreated specimen, some tiny peeled-off particles were observed on the surface, owing to a true contact area and an initial surface roughness, which was smoother than that of the UNSM-treated specimen. The specific wear rate was quantified according to the cross-sectional profiles of each wear track and wear test conditions. Results revealed that the specific wear rates of the untreated and UNSM-treated bulk and 3D-printed specimens were $5.6 \times 10^{-6} \text{ mm}^3/\text{Nm}$, $3.4 \times 10^{-6} \text{ mm}^3/\text{Nm}$, $2.4 \times 10^{-6} \text{ mm}^3/\text{Nm}$, and $1.3 \times 10^{-6} \text{ mm}^3/\text{Nm}$, respectively. The bulk specimens evidently had a lower wear resistance than the 3D-printed specimens. The wear mechanism of the untreated specimens was adhesive wear, occurring mainly due to the plastic deformation during sliding contact, as shown in Figure 9a,c. It was also observed that the wear track of the UNSM-treated specimens showed no cracks, whereas the presence of micro-cracks (shown by arrows) inside the wear track of the untreated ones were confirmed by high-magnification SEM images, as shown in Figure 9b,d. Abrasion wear could be observed on the surface of the UNSM-treated specimens, which was attributed mainly to the detachment of the initial asperities derived from the rough surface induced by the UNSM treatment. The adhesive wear can be explained by the fact that the oxide layer on the asperities is broken up easily due to the contact stress, resulting in direct metal-to-metal contact [36,37]. Thus, the wear track of each specimen was subjected to EDS to investigate the chemical state of the wear track, as shown in Figure 10. The presence of oxides was also detected, and was found to affect the friction and wear mechanisms as well, as shown in Figure 10a,b, which developed during the dry sliding of the materials in relative motion. Oxidative wear was found to be dominant for the 3D-printed specimens, as shown in Figure 10c,d, but the level of oxidation was much higher at the interface where the untreated specimen came into contact with the counter surface compared to the interface where the UNSM-treated specimen came into contact with the counter surface under dry conditions. Moreover, the presence of oxide films at the interface could be responsible for the lack of steady-state behavior of the friction over sliding time shown in Figure 9. Hence, the oxide layer was not particularly beneficial in reducing the friction coefficient, while it also deteriorated the wear resistance of the materials [38]. In addition, it is well known that several types of wear mechanisms take place for metallic materials during wear processing simultaneously, where a great amount of carbon and oxygen can be formed during wear processing in steels. In general, a carbon-rich tribo-layer can be formed at the contact interface during sliding [39].

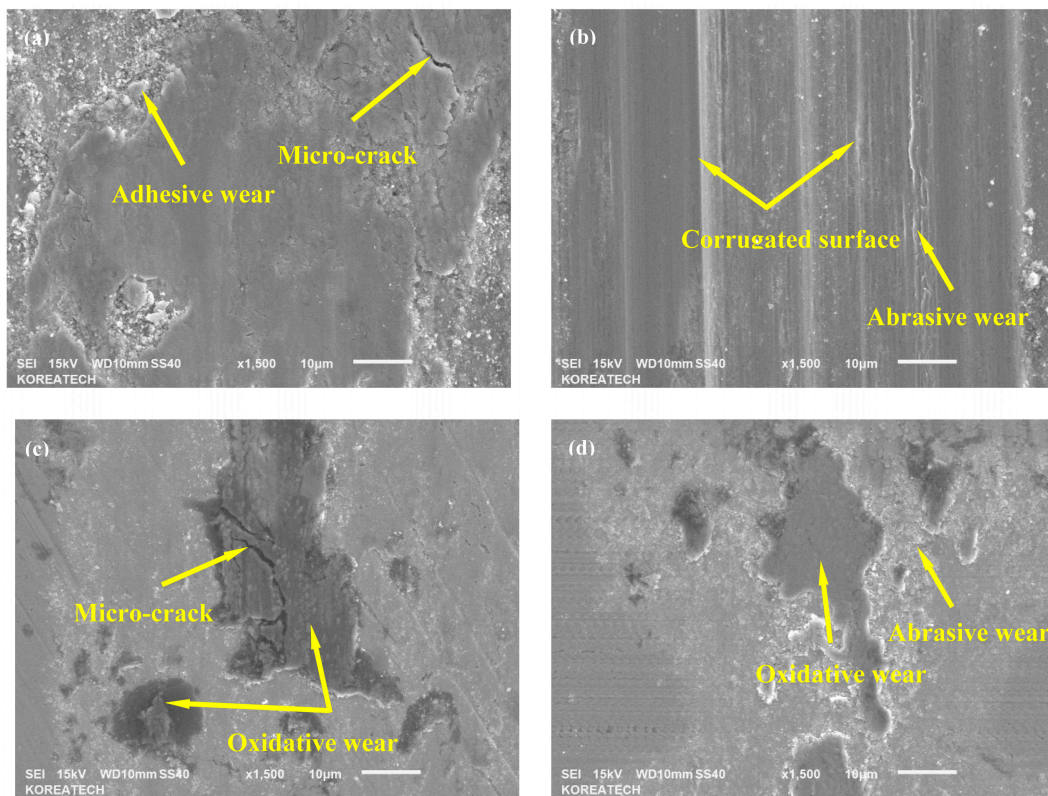


Figure 9. High-magnification SEM images of the bulk (a,b) and 3D-printed (c,d) AISI H13 tool steel specimens before and after UNSM treatment.

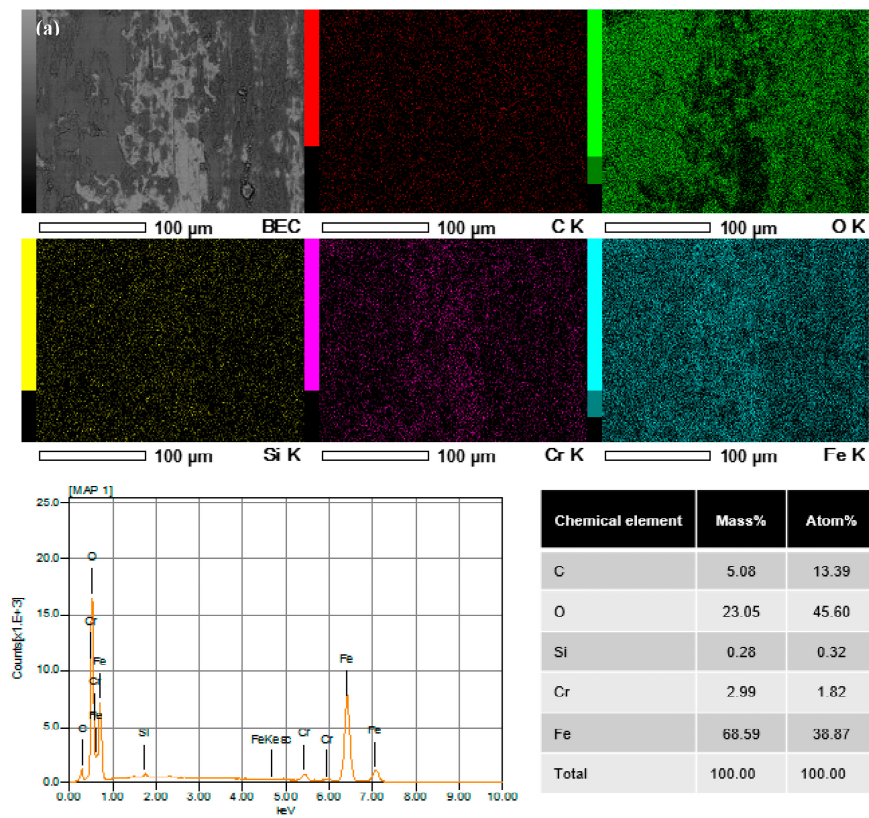


Figure 10. Cont.

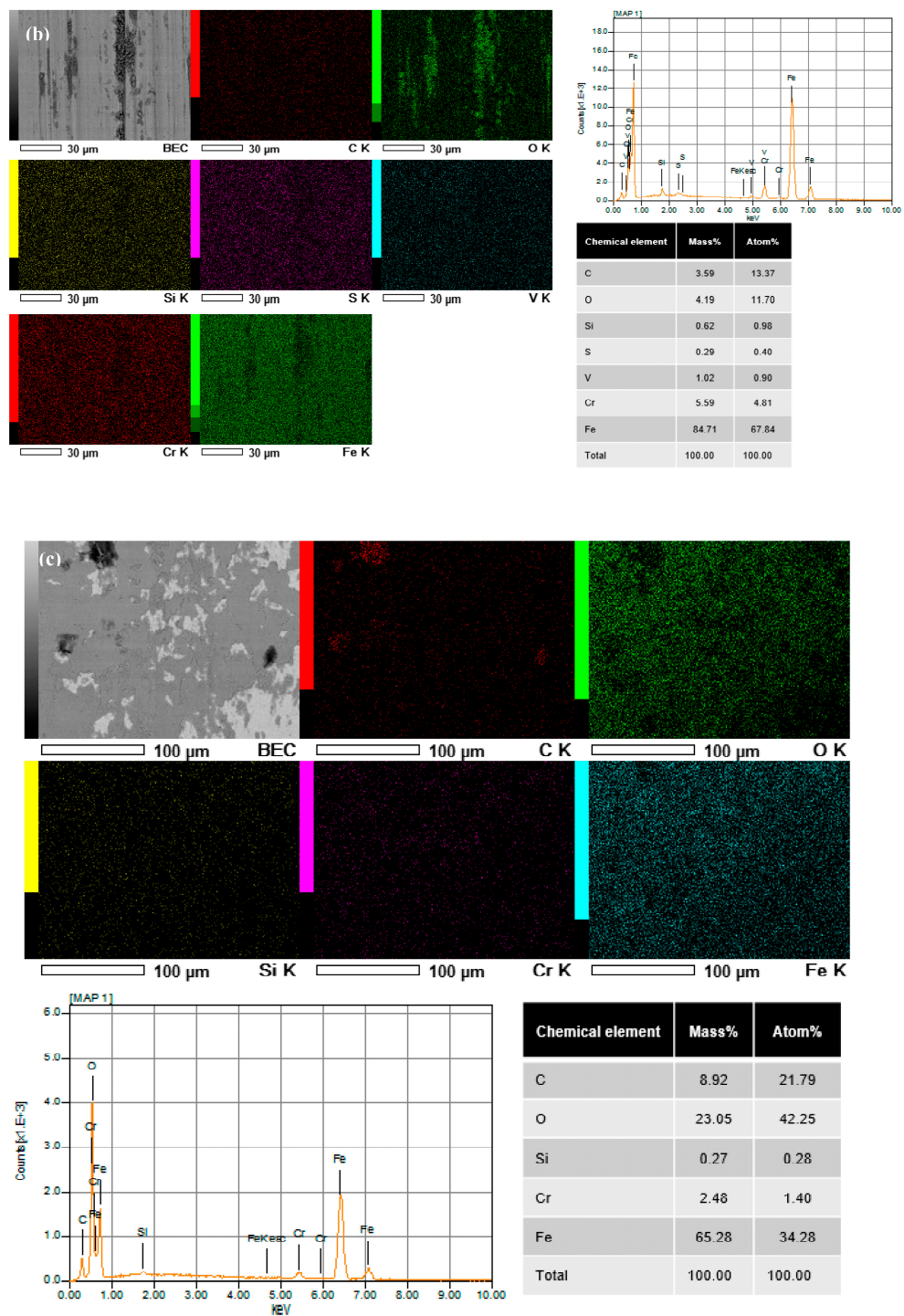


Figure 10. Cont.

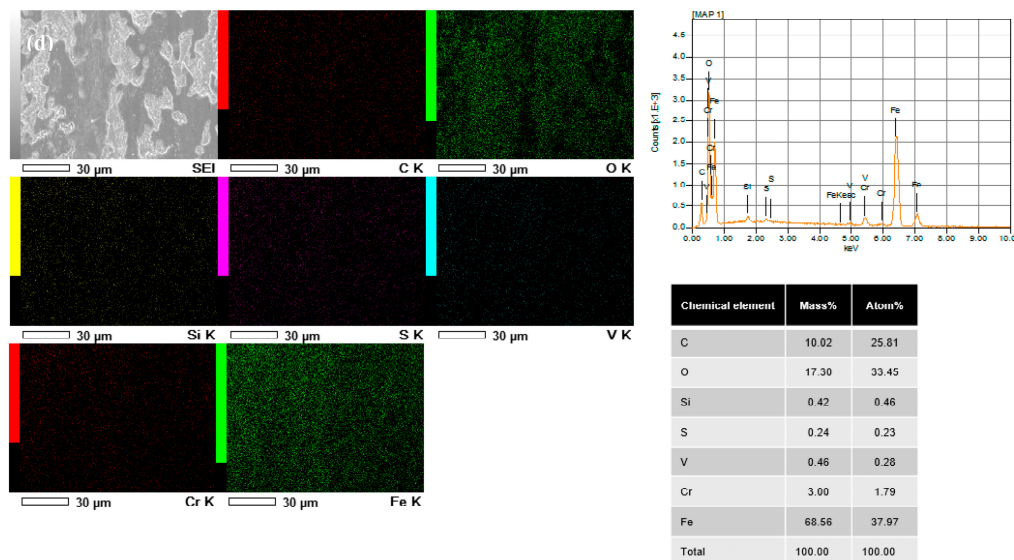


Figure 10. Energy-dispersive X-ray spectroscopy (EDX) spectra of the wear track of the bulk (a,b) and 3D-printed (c,d) AISI H13 tool steel specimens before and after UNSM treatment.

4. Conclusions

In this study, two different AISI H13 tool steels—bulk and 3D-printed—were subjected to UNSM treatment. The surface roughness, surface hardness, friction and wear behavior, and microstructural evolution in terms of the grain size and number of fractions were investigated for the specimens and compared with the results obtained for the corresponding untreated specimens. According to the experimental results, the followings conclusions can be drawn:

- (1) The average grain size of the as-received specimen was in the range of 5–30 μm in the longitudinal direction, which was refined to very fine grains with sizes in the range of 1–10 μm in the longitudinal direction after UNSM treatment. LAGB and HAGB of the bulk specimens were about 21% and 79%, and those of the 3D-printed specimens were about 8% and 92%, respectively.
- (2) The average surface roughness of the bulk specimen increased after UNSM treatment from 0.445 to 0.563 μm , while no significant difference was observed for the average surface roughness of the 3D-printed untreated and UNSM-treated specimens, with observed values of 0.451 and 0.454 μm , respectively. The surface hardness of the as-received and UNSM-treated bulk and 3D-printed specimens increased from 21 to 34 HRC and 60 to 65 HRC, respectively.
- (3) The friction coefficient of the untreated specimen in the running-in and steady-state periods was found to be higher than that of the UNSM-treated specimen by about 14%. For the 3D-printed specimens, the friction coefficient increased rapidly at the onset of sliding, where the UNSM-treated specimen showed a higher decrease rate than the untreated one by about 20%. The specific wear rates of the untreated and UNSM-treated bulk and 3D-printed specimens were $5.6 \times 10^{-6} \text{ mm}^3/\text{Nm}$, $3.4 \times 10^{-6} \text{ mm}^3/\text{Nm}$, $2.4 \times 10^{-6} \text{ mm}^3/\text{Nm}$, and $1.3 \times 10^{-6} \text{ mm}^3/\text{Nm}$, respectively.

Hence, this work demonstrated the capability of achieving excellent mechanical and tribological properties for AISI H13 tool steel for industrial applications. In the near future, it is expected that UNSM processed 3D-printed metallic materials can be replaced bulk metallic materials because of their economic advantages.

Acknowledgments: This work was supported by the Industrial Strategic Technology Development Program (20165020301430) funded by the Ministry of Trade, Industry, and Energy (MI, Korea).

Author Contributions: Yongho Jeon and In-Sik Cho designed the experiments; Hyung-Gyu Lee and Moon Gu Lee performed the experiments; Chang-Soon Lee, Chang-Ha Choi, and Yongho Jeon analyzed the data. In-Sik Cho and Yongho Jeon wrote the manuscript.

Conflicts of Interest: The authors declare no conflicts of interest.

References

1. Li, S.; Wu, X.; Chen, S.; Li, J. Wear resistance of H13 and a new hot-work die steel at high temperature. *J. Mater. Eng. Perform.* **2016**, *25*, 2993–3006. [[CrossRef](#)]
2. Marashi, J.; Yakushina, E.; Xirouchakis, P.; Zante, R.; Foster, J. An evaluation of H13 tool steel deformation in hot forging conditions. *J. Mater. Process. Technol.* **2017**, *246*, 276–284. [[CrossRef](#)]
3. Lee, J.Y.; An, J.; Chul, C.K. Fundamentals and applications of 3D printing for novel materials. *Appl. Mater. Today* **2017**, *7*, 120–133. [[CrossRef](#)]
4. Baletti, C.; Ballarin, M.; Guerra, F. 3D printing: State of the art and future perspectives. *J. Cult. Herit.* **2017**, *26*, 172–182. [[CrossRef](#)]
5. Chen, L.Y.; Huang, J.C.; Lin, C.H.; Pan, C.T.; Chen, S.Y.; Yang, T.L.; Lin, D.Y.; Lin, H.K.; Jang, J.S.C. Anisotropic response of Ti-6Al-4V alloy fabricated by 3D printing selective laser melting. *Mater. Sci. Eng. A* **2017**, *682*, 389–395. [[CrossRef](#)]
6. Geissbauer, R.; Wunderlin, J.; Lehr, J. The Future of Spare Parts of 3D: A look at the challenges and opportunities of 3D printing. *Strategy*, 30 January 2017.
7. Wong, K.V.; Hernandez, A. A review of additive manufacturing. *ISRN Mech. Eng.* **2012**, *2012*. [[CrossRef](#)]
8. Lipson, H.; Kurman, M. *Fabricated: The New World of 3D Printing: The Promise and Peril of a Machine That Can Make (Almost) Anything*; John Wiley & Sons, Inc.: Lebanon, IN, USA, 2013.
9. Bremen, S.; Meiners, W.; Diatlov, A. Selective laser melting. *Laser Technol. J.* **2012**, *9*, 33–38. [[CrossRef](#)]
10. Slotwinski, J.A.; Garboczi, E.J.; Hebenstreit, K.M. Porosity measurement and analysis for metal additive manufacturing process control. *J. Res. Natl. Inst. Stand. Technol.* **2014**, *119*, 494–506. [[CrossRef](#)] [[PubMed](#)]
11. Frazier, W.E. Metal additive manufacturing: A review. *J. Mater. Eng. Perform.* **2014**, *23*, 1917–1931. [[CrossRef](#)]
12. AlMangour, B.; Grzesiak, D.; Yang, J.M. Selective laser melting of TiB₂/H13 steel nanocomposites: Influence of hot isostatic pressing post-treatment. *J. Mater. Process. Technol.* **2017**, *244*, 344–353. [[CrossRef](#)]
13. Yang, H.; Wu, X.; Cao, G.; Yang, Z. Enhanced boronizing kinetics and high temperature wear resistance of H13 steel with boriding treatment assisted by air blast shot peening. *Surf. Coat. Technol.* **2016**, *307*, 506–516. [[CrossRef](#)]
14. Yeh, S.H.; Chiu, L.H.; Chuang, T.L.; Wu, C.Y. Thermal fatigue behavior evaluation of shot-peened JIS SKD61 hot-work mold steel. *Mater. Trans.* **2013**, *54*, 1053–1056. [[CrossRef](#)]
15. Sabirov, I.; Enikeev, N.A.; Murashkin, M.Y.; Valiev, R.Z. *Bulk Nanostructured Materials with Multifunction Properties*; SpringerBriefs Materials; Springer: New York, NY, USA, 2015.
16. Cho, K.T.; Song, K.; Oh, S.H.; Lee, Y.K.; Lee, W.B. Surface hardening of shot peened H13 steel by enhanced nitrogen diffusion. *Surf. Coat. Technol.* **2013**, *232*, 912–919. [[CrossRef](#)]
17. Pinkerton, A.J.; Wang, W.; Li, L. Component repair using laser direct metal deposition. *Part B J. Eng. Manuf.* **2008**, *222*, 827–836. [[CrossRef](#)]
18. Chen, J.; Xue, L. Laser cladding of CPM tool steels on hardened H13 hot-work steel for low-cost high-performance automotive tooling. *J. Mater. Sci.* **2012**, *64*, 688–693. [[CrossRef](#)]
19. Amanov, A.; Cho, I.S.; Pyoun, Y.S.; Lee, C.S.; Park, I.G. Micro-dimples surface by ultrasonic nanocrystal surface modification and its tribological effects. *Wear* **2012**, *286–287*, 136–144. [[CrossRef](#)]
20. Amanov, A.; Cho, I.S.; Kim, D.E.; Pyun, Y.S. Fretting wear and friction reduction of CP titanium and Ti-6Al-4V alloy by ultrasonic nanocrystalline surface modification. *Surf. Coat. Technol.* **2012**, *207*, 135–142. [[CrossRef](#)]
21. Amanov, A.; Pyun, Y.S.; Sasaki, S. Effects of ultrasonic nanocrystalline surface modification (UNSM) technique on the tribological behavior of sintered Cu-based alloy. *Tribol. Int.* **2014**, *74*, 187–197. [[CrossRef](#)]
22. Amanov, A.; Lee, S.W.; Pyun, Y.S. Low friction and high strength of 316L stainless steel tubing for biomedical application. *Mater. Sci. Eng. C* **2017**, *71*, 176–185. [[CrossRef](#)] [[PubMed](#)]
23. Amanov, A.; Cho, I.S.; Park, I.G.; Pyun, Y.S. The migration of spheroidal cementite towards the surface in nanostructured AISI 52100 steel. *Mater. Lett.* **2016**, *174*, 142–145. [[CrossRef](#)]
24. Shackelford, J. *Introduction to Materials Science for Engineers*; Pearson: San Francisco, CA, USA, 2015.

25. Valiev, R.Z.; Zhilyaev, A.P.; Langdon, T.G. *Bulk Nanostructured Materials: Fundamentals and Applications*; John Wiley & Sons: New York, NY, USA, 2013.
26. Amanov, A.; Cho, I.S.; Pyun, Y.S. Microstructural evolution and surface properties of nanostructured Cu-based alloy by ultrasonic nanocrystalline surface modification. *Appl. Surf. Sci.* **2016**, *388*, 185–195. [[CrossRef](#)]
27. Greiner, C.; Merz, T.; Braun, D.; Codrignani, A.; Magagnato, F. Optimum dimple diameter for friction reduction with laser surface texturing: The effect of viscosity gradient. *Surf. Topogr. Metrol. Prop.* **2015**, *3*, 044001. [[CrossRef](#)]
28. Amanov, A.; Pyun, Y.S.; Zhang, B.; Park, J.H.; Nohava, J. Preliminary study of the effect of micro-scale dimple size on friction and wear under oil-lubricated sliding conditions. *Tribol. Int.* **2011**, *6*, 284–290.
29. Sames, W.J.; List, F.A.; Pannala, S.; Dehoff, R.R.; Babu, S.S. The metallurgy and processing science of metal additive manufacturing. *Int. Mater. Rev.* **2016**, *61*, 315–360. [[CrossRef](#)]
30. Hanamura, T.; Qui, H. *Analysis of Fracture Toughness Mechanism in Ultra-Fine Grained Steels*; NIMS Monographs; Springer: Ibaraki, Japan, 2014.
31. Callister, W.D.; Rethwisch, D.G. *Materials Science and Engineering: An Introduction*; John Wiley & Sons: New York, NY, USA, 2013.
32. Amanov, A.; Sasaki, S.; Pyun, Y.S. Frictional behavior of duplex nano-corrugated and nanostructured Cu alloy produced by UNSM. *Procedia Eng.* **2013**, *68*, 491–496. [[CrossRef](#)]
33. Johnson, K.K. *Contact Mechanics*, 9th ed.; Cambridge University Press: Cambridge, UK, 2003.
34. Pereira, D.; Gandra, J.; Pamies-Teixeira, J.; Miranda, R.M.; Vilaca, P. Wear behaviour of steel coatings produced by friction surfacing. *J. Mater. Process. Technol.* **2014**, *214*, 2858–2868. [[CrossRef](#)]
35. Amanov, A.; Penkov, O.V.; Pyun, Y.S.; Kim, D.E. Effects of ultrasonic nanocrystalline surface modification on the tribological properties of AZ91D magnesium alloy. *Tribol. Int.* **2012**, *54*, 106–113. [[CrossRef](#)]
36. Fontavlo, G.A.; Hummer, R.; Mitterer, C.; Sammt, K.; Schemmel, I. Microstructural aspects determining the adhesive wear of tool steels. *Wear* **2006**, *260*, 1028–1034.
37. Mesquita, R.A. *Tool Steels: Properties and Performance*; CRC Press: Boca Raton, FL, USA, 2017.
38. Stachowiak, G.W.; Batchelor, A.W. *Engineering Tribology*, 3rd ed.; Elsevier: Oxford, UK, 2005.
39. Ulutan, M.; Celik, O.N.; Gasan, H.; Er, U. Effect of different surface treatment methods on the friction and wear behavior of AISI 4140 steel. *J. Mater. Sci. Technol.* **2010**, *26*, 251–257. [[CrossRef](#)]



© 2017 by the authors. Licensee MDPI, Basel, Switzerland. This article is an open access article distributed under the terms and conditions of the Creative Commons Attribution (CC BY) license (<http://creativecommons.org/licenses/by/4.0/>).